The State Scientific Center of Russia

The Budker Institute of Nuclear Physics

SB RAS

R.R.Akhmetshin, G.A.Aksenov, E.V.Anashkin,
V.M.Aulchenko, B.O.Baibusinov, V.S.Banzarov,
L.M.Barkov, S.E.Baru, A.E.Bondar, V.V.Danilov,
S.I.Eidelman, G.V.Fedotovich, N.I.Gabyshev,
A.A.Grebeniuk, D.N.Grigoriev, P.M.Ivanov,
B.I.Khazin, I.A.Koop, A.S.Kuzmin, I.B.Logashenko,
A.P.Lysenko, A.V.Maksimov, Yu.I.Merzlyakov,
V.A.Monitch, I.N.Nesterenko, V.S.Okhapkin,
E.A.Perevedentsev, A.A.Polunin, E.V.Popkov,
V.I.Ptitzyn, T.A.Purlatz, S.I.Redin,
N.I.Root, A.A.Ruban, N.M.Ryskulov,
Yu.M.Shatunov, A.E.Sher, M.A.Shubin, B.A.Shwartz,
V.A.Sidorov, A.N.Skrinsky, V.P.Smakhtin,
I.G.Snopkov, E.P.Solodov, A.I.Sukhanov, V.M.Titov,
Yu.V.Yudin, V.G.Zavarzin, D.H.Brown, J.P.Miller,
B.L.Roberts, W.A.Worstell, J.A.Thompson,
C.M.Valine, P.B.Cushman, S.K.Dhawan, V.W.Hughes

MEASUREMENT OF ϕ-MESON PARAMETERS WITH CMD-2 DETECTOR AT VEPP-2M COLLIDER

Budker INP 95-35

НОВОСИБИРСК

MEASUREMENT OF ϕ-MESON PARAMETERS WITH CMD-2 DETECTOR AT VEPP-2M COLLIDER

R.R.Akhmetshin, G.A.Aksenov, E.V.Anashkin, V.M.Aulchenko, B.O.Baibusinov, V.S.Banzarov, L.M.Barkov, S.E.Baru, A.E.Bondar, V.V.Danilov, S.I.Eidelman, G.V.Fedotovich, N.I.Gabyshev, A.A.Grebeniuk, D.N.Grigoriev, P.M.Ivanov, B.I.Khazin, I.A.Koop, A.S.Kuzmin, I.B.Logashenko, A.P.Lysenko, A.V.Maksimov, Yu.I.Merzlyakov, V.A.Monitch, I.N.Nesterenko, V.S.Okhapkin, E.A.Perevedentsev, A.A.Polunin, E.V.Popkov, V.I.Ptitzyn, T.A.Purlatz, S.I.Redin, N.I.Root, A.A.Ruban, N.M.Ryskulov, Yu.M.Shatunov, A.E.Sher, M.A.Shubin, B.A.Shwartz, V.A.Sidorov, A.N.Skrinsky, V.P.Smakhtin, I.G.Snopkov, E.P.Solodov, A.I.Sukhanov, V.M.Titov, Yu.V.Yudin, V.G.Zavarzin,

Budker Institute of Nuclear Physics,
Novosibirsk, 630090, Russia

Brown D.H., Miller J.P., Roberts B.L., Worstell W.A.

Boston University

Thompson J.A., Valine C.M.

University of Pittsburgh

Cushman P.B.,

University of Minnesota

Dhawan S.K., Hughes V.W.

Yale University

Abstract

Results of the measurement of the ϕ-meson parameters with the general purpose detector CMD-2 at the upgraded e^+e^- collider VEPP-2M at Novosibirsk are presented. This is the first measurement of the four major ϕ decay modes in a single experiment. The results are consistent with previous measurements, and have errors comparable to the current world averages.

1 Introduction

The VEPP-2M collider at the Budker Institute of Nuclear Physics in Novosibirsk, Russia, shown in Figure 1 covers the center of mass energy range from the two pion threshold up to 1400 MeV [1]. Experiments at this collider yielded a number of important results in e^+e^- physics, including the most precise pion form factor measurements [2] and studies of the ϕ, ω, and ρ meson decays [3, 4]. During 1988-92 it was upgraded to allow higher positron currents and injection of the electron and positron beams directly at the beam energy, rather than at lower energies and acceleration after injection. After installation of the new booster, VEPP-2M has peak luminosity $L \approx 5. \times 10^{30} cm^{-2} s^{-1}$ at 40 mA per beam at the ϕ center of mass energy.

In this paper we present results on the four major decay modes of the ϕ: $\phi \to K_S K_L$, $\phi \to K^+K^-$, $\phi \to \eta\gamma$, and $\phi \to \pi^+\pi^-\pi^0$ based on about $290 nb^{-1}$ of the data collected at the ϕ-meson during the 1992 runs.

2 The Detector

The CMD-2 detector shown in Figure 2 is situated in one of the interaction regions of VEPP-2M. It is a general purpose detector with a drift chamber and proportional Z-chamber inside an axial magnetic field, as well as a barrel (CsI) calorimeter and muon range system, both outside the field [5]. A BGO endcap calorimeter has now been added but was not in place for the data discussed here.

2.1 Tracking system

The tracking system of the detector consists of a cylindrical drift chamber (DC) [6] with 80 jet-type drift cells arranged in three superlayers with wires parallel to the beam, and a double layer multiwire proportional chamber with cathode and anode readout [7] (called the Z-chamber, or ZC, and with wires oriented along the beam axis) placed behind the DC. The outer radius of the DC is 30 cm, and the length of the sensitive volume is 42 cm. The Z-chamber wires are 80 cm long and cover bigger solid angle, than DC. Both chambers are mounted inside a thin (0.4 X_0) superconducting solenoid with an azimuthally symmetric magnetic field of 1.0 T [8]. The uniformity of the field is better than 1.5% over the DC volume. All three coordinates of the charged particle track in the DC are determined from the wire radius, the drift time and charge division, with about 250 μ resolution transverse to the beam and 0.4-0.5 cm longitudinally. The momentum resolution seen is 3-4% for 200 MeV/c pions from neutral kaon decays and about 6% for 500 MeV electrons from e^+e^- elastic scattering (Bhabha) events. Figure 3 shows the DC dE/dx response for the collinear events at the ϕ-meson energy for minimum ionizing particles (shaded) and slow kaons, selected by momenta. This parameter was used to reduce background of slow charged kaons to pions from other ϕ decays.

The Z-chamber anode signals are used in the trigger. The required time resolution of less than 60 ns is determined by the VEPP-2M bunch crossing frequency. For the fast gas mixture of freon-14 (CF_4) with a 10% admixture of isobutane, averaged over four hits, a time jitter of around 5 ns is seen. The Z-resolution from the cathode information reconstruction is presented in Figure 4. The resolution averaged over all track angles was found to be 0.05 cm. The Z-chamber presents 2.4% radiation lengths to a passing particle.

2.2 Barrel Calorimeter

The CsI barrel calorimeter [9], 8.1 X_0 deep, is placed outside the solenoid. The calorimeter consists of 8 octants. Each octant contains 112 CsI crystals doped with Na or Tl and arranged in 7 linear modules of 16 crystals each. Five of these modules are constructed of the rectangular parallelepiped blocks with a $6 \times 6 \times 15$ cm^3 size while the two edge modules consist of crystals with a special shape to assure close contact of the octants while keeping approximately the same scintillator thickness in these regions. The readout was performed by photomultipliers. The calorimeter gives an angular resolution of 0.02-0.03 radians and an energy resolution of 8-10% (FWHM/2.36) in

the energy range 100-500 MeV, in good agreement with a simulation. The Bhabha events are used for calibration to obtain this resolution.

Figure 5 presents the distribution of the energy deposition of one cluster in the calorimeter for selected events with two collinear tracks. A low energy peak corresponds to minimum ionizing particles ($e^+e^- \to \mu^+\mu^-, \pi^+\pi^-$ and cosmic background) while the high energy peak is due to Bhabha events.

2.3 Range system

The muon range system consists of two double layers of streamer tubes operating in a self-quenching streamer mode and is aimed at separation of pions and muons [10].

The inner part of the system is placed inside the iron yoke just after the CsI calorimeter and covers 55 % of the solid angle. It consists of 8 modules with 48 streamer tubes each. For a pion the probability to hit the system and imitate a muon is 0.35 for a single track or 0.1 for collinear tracks. The outer part is placed outside the yoke and covers 48% of the solid angle. Five upper modules have 32 tubes each while three lower have 24 tubes each. The muon and pion separation in the outer system is characterized by probabilities of 0.1 and 0.01 for single and collinear tracks respectively.

The spatial resolution determined with the help of cosmic rays is 50-70 mm along a wire and the detection efficiency of the double layer is more than 99%.

2.4 Tracking processor and Trigger

The trigger [11] is started by signals from the Z-chamber. The tracking processor generates a "common stop" signal after finding one or more tracks in the two inner sectors of the drift chamber. The outer sector is not used, to allow a larger solid angle for the trigger tracks. If there is no "common stop" signal, the stored digital information is cleared after 1.25 μsec.

A pretrigger from the Z-chamber gives a rate of 10-16 kHz, dominated by background beam interactions and sensitive to the tuning of the accelerator. These data were taken with a trigger requiring one charged track passing near the beam-beam interaction point, which suppresses backgrounds by a factor of 60-100 to a level of 100-300 Hz. An additional requirement of 60 MeV energy deposition in the barrel calorimeter reduces the triggered data by an additional factor of 10.

This loose trigger still includes about 90% background events, of which about half are events with only one track and one cluster. These events arise

from background beam-beam, beam-wall, and beam-gas interactions.

The data acquisition system uses a PDP-11 computer and a custom built AP32 processor for the online control [12], with recording to the EXABYTE tapes with the 25Hz output limit for 1 kbyte average event size. For later data taking the DAQ limit was increased to 50 Hz by specialized optimization of the code.

Since the acquisition of these data, an additional (third) trigger level, coded in the AP32 processor, has been introduced, reducing the output by another factor of 2-3.

3 Analysis

3.1 Detector Properties and Reconstruction Efficiencies

The detection and reconstruction efficiencies were determined from a combination of simulated event studies, special dedicated runs to check trigger efficiency, studies of the correlations between responses of the detector subsystems and experimental event distributions.

The MC simulation of the detector is based on GEANT code [13], and a sufficiently large sample of each channel of interest has been generated (from 6k $\eta\gamma$ to 250k K^+K^-). In addition to the efficiencies in the completely operational (ideal) detector, there are known hardware trigger and detector inefficiencies, whose effects are estimated separately. These inefficiencies were studied as a function of the run number using a comparison of the experimental distributions and simulation and were in the range from 4 to 35 percents.

The resulting efficiencies with their statistical errors are given as ϵ_{rec} in Tables I-V along with other quantities, described in the next sections. Systematic uncertainties were estimated separately by two different procedures of selecting Bhabha events and were found to be about 2%. They were included in the overall systematic uncertainty of the cross section in each energy point.

Special dedicated runs were used to estimate trigger efficiency for each studied channel. One set of these runs uses only the trackfinder to trigger the detector in order to study the calorimeter efficiency. Another set of runs uses the calorimeter as the main trigger and the signal from the trackfinder is used for efficiency studies. These efficiencies were calculated separately for each channel. The neutral and charged parts of the trigger efficiency as well as their combination are presented in Table VI for each channel. The last

line shows efficiencies for the given channel, normalized to the efficiency for collinear events.

For the low statistics $\eta\gamma$ channel the trigger efficiencies were taken to be the same as for three pions.

Errors from these trigger efficiencies were included into the overall systematic uncertainty of the peak cross section and branching ratio for each channel.

3.2 Collinear Event Selection and Luminosity Determination

The luminosity is initially determined roughly from the BGO crystal double bremsstrahlung monitors [14]. It is determined more precisely using the observed number (N_{coll}) of the collinear e^+e^-, $\mu^+\mu^-$, and $\pi^+\pi^-$ events:

$$L = \frac{N_{coll}}{\sigma_{coll}\epsilon_{rec}\epsilon_{trig}},$$

where

$$\sigma_{coll} = \sigma_{ee}(1+\delta_{rad,e}) + \sigma_{\mu\mu}(1+\delta_{rad,\mu}) + \sigma_{\pi\pi}(1+\delta_{rad,\pi})$$

is the sum of the Born cross sections for the collinear events with radiative corrections, obtained by Monte-Carlo simulation of the ideal detector; ϵ_{rec} is the reconstruction efficiency for collinear events; ϵ_{trig} is the trigger efficiency. The cross sections for electrons and muons are calculated from quantum electrodynamics, and the pion cross sections are obtained by using the values of form factor as previously measured [2].

The criteria for the collinear events used in determining the luminosity are:

1. Average momentum of the two charged tracks is greater than 240 MeV/c, and the transverse momentum of each track is less than 800 MeV/c. Figure 6a shows the average momentum distribution for collinear events.

2. Azimuthal angle difference ($\Delta\phi$) is less than 0.1 radian. Figure 6c shows the $\Delta\phi$ distribution, and indicates an angular resolution of about one milliradian.

3. Tracks is nearly perpendicular to the beam: θ between 1. and 2.14 radians. Figure 6b shows the polar angle distribution for collinear events,

mostly determined by Bhabha events, shown by the dashed histogram, where an additional cut on cluster energy has been applied.

4. Number of points on each track at least 6.

5. Radial distance from the nominal collision point to the vertex is less than 0.5 cm. Figure 6d shows the distribution of the radial distance of the two-track vertex from the nominal collision point.

After these cuts the cross section for the collinear events is about 530 nb^{-1}. To get a number of the collinear events, as well as for each other channel described below, a subtraction was made in the Z-vertex distribution, to remove cosmic ray background. The distributions of the Z-vertices for different channels are shown in Figure 7. The number of selected collinear events, reconstruction efficiency, calculated cross section and luminosity for each energy point, are given in Table I. Only statistical errors are listed.

Beside with the systematic uncertainty in the determination of ϵ_{rec} for individual energy point (see section above), the general systematic error in the luminosity measurement come from the uncertainty in the fiducial solid angle and has been estimated as 3%.

3.3 Selection of Charged Kaon events

The most common decay channel of the ϕ-meson is to two charged kaons. However, the final kaons have a low kinetic energy, not sufficient to go through the Z-chamber. The Z-chamber can be fired only by secondary particles from nuclear interactions or decays of stopped kaons. The CMD-2 trigger demands at least one charged track in both the drift chamber and the Z-chamber, and our studies of the K_L interactions in the calorimeter [15] indicate that the present GEANT simulation of low momentum kaon nuclear interactions is not sufficiently accurate to allow its use in the determination of absolute efficiencies. Therefore we use only K^+K^- events in which one kaon decays in flight within 6 cm radially from the interaction region. Although the long decay length of the kaons (about 50 cm at these energies) makes this a strong requirement which severely reduces the number of events, at least one particle is guaranteed to be energetic enough to make a trigger. An example of this kind of event is shown in Figure 8.

The cuts used in the selection of the event sample are:

1. The momentum of the charged decay product in the kaon rest frame is between 110 and 360 MeV/c.

2. The opening angle between the decay product and the kaon is in the interval 0.15 - 3.0 radians.

3. The momentum of the kaon is not more than 40 MeV/c exceeds the momentum calculated from the beam energy and kaon mass.

4. The angle of the secondary muon or pion as well as the kaon angle with respect to the z-axis is between 1.0 and 2.14 radians to guarantee hitting the barrel calorimeter and provide trigger.

5. The decay vertex is between 0.5 cm and 6 cm from the center of the detector radially, excluding $\pm$0.3 cm around beam pipe, and within 10 cm of the center of the detector longitudinally.

Figure 9a represents a histogram of the reconstructed momentum of secondary particles from charged kaons decaying at rest. From the standard branching ratios one expects 21% in the mode $\pi\pi^0$ and 64% in the mode $\mu\nu$. Two peaks from muons and pions are clearly seen. Figure 9b gives the radial distance of the decay from the nominal collision point. A peak from the nuclear interacting kaons at the Be pipe is seen.

The number of events in both decay modes ($\pi\pi^0$ and $\mu\nu$) is determined from a fit to two Gaussians centered at 205 MeV/c and 236 MeV/c respectively with subtracting a smooth background, which is caused by the three-body decays.

The Monte Carlo detection efficiency averaged over the ϕ-meson region for the ideal detector is 0.0203$\pm$0.0003 and slightly decreases with energy.

The detailed efficiencies and the number of events selected at each energy are shown in Table II. The total number of K^+K^- events, with one identified decay, is 2913.

3.4 Selection of $K^0_SK^0_L$ Events

The K_SK_L decay mode has a branching ratio of about 34%. An example of a K_SK_L double-decay event is shown in Figure 10. Usually only the K_S decays were seen. The ϕ-meson decays into K_SK_L with subsequent decay $K_S \to \pi^+\pi^-$ were selected with the help of the parameters shown in Figure 11. It was assumed that charged tracks are pions and imposed cuts are enumerated below :

1. Two pions are seen in the drift chamber making a vertex within 3 cm of the beam radially.

2. The average momentum of two charged pions (supposedly coming from the K_S decay) is between 180 and 250 MeV/c.

3. The missing momentum in the drift chamber is between 60 and 150 MeV/c.

4. M_{inv}, the invariant mass of the two charged pions is between 450 and 550 MeV/c^2.

5. The momentum of each of two charged pions is between 140 and 290 MeV/c.

6. The angles of the pions with respect to the z-axis are between 0.8 and 2.34 radians.

To obtain the number of events used in the cross section calculations, cosmic ray events were removed by a subtraction of a smooth background in z from the z-vertex distributions demonstrated in Figure 7b,d. This background was low at the resonance (Figure 7b) and dominated at the energy points aside of the resonance peak (Figure 7d).

The ideal detector efficiency for K_S with the above cuts was found from the simulated events to range from 37.2% at a center of mass energy of 1008 MeV, to 34.8% at the highest energy of 1028.2 MeV. The average efficiency over the ϕ-meson region is determined to be 0.359 $\pm$ 0.002. The detailed efficiencies and number of events selected at each energy point are given in Table III.

The total sample of events in this channel is 40,644 with a reconstructed K_S. About 400 are with both K_S and K_L separately reconstructed.

3.5 Selection of $\pi^+\pi^-\pi^0$ Events

The three-pion final state was searched for in a sample of events with two charged tracks. The tracks assumed to be pions must satisfy the following requirements:

1. The vertex formed by the charged tracks is within 0.5 cm of the beam position radially.

2. The momentum of each charged track is less than 500 MeV/c.

3. The missing momentum (of the supposed neutral pion) is between 100 and 500 MeV/c.

4. The missing mass squared (of the supposed neutral pion) is between -100000 and 120000 MeV^2/c^4.(Figure 12a)

5. The average momentum of the two charged tracks is between 230 and 400 MeV/c. (Figure 12c)

6. The angles of the pions with respect to the z-axis are between 0.8 and 2.34 radians.

7. The azimuthal angular acollinearity is greater than 0.15 radians, and $\Delta\psi$ (the opening angle between the two charged tracks) is less than 2.5 radians to remove $K_S \to \pi^+\pi^-$ background.

An example of a reconstructed three pion event is shown in Figure 13. As well as for the other channels, subtraction in z removes cosmic ray background (Figure 7c) which is very low for this channel. The detailed efficiencies and number of events selected at each energy point are given in Table IV. The total number of events reconstructed in this channel is 11,761.

The requirement that the neutral pion be reconstructed from the photon showers in the CsI calorimeter was not applied, because 1) it reduced the number of events by a factor of two due to the solid angle of the CsI calorimeter, and 2) the fraction of the reconstructed π^0 was different for simulated and real events. The last item is under study now and believed to be due to the presence of some number of background clusters in real data. Nevertheless, events with good reconstructed neutral pions were used to estimate nonresonance background coming from four pion production. The events where a π^0 was reconstructed with a momentum matching the missing momentum from the charged particles have almost no background. The ratio of the number of events without a reconstructed π^0 to the number with found π^0 at the top of the ϕ-meson was 2.2. At the energy point 497 MeV per beam, this ratio was 4.2 and 37 events with reconstructed π^0 were found. Applying the ratio at the ϕ-meson mass to the 37 found events, gave an estimate of 74$\pm$20 background events presented in the 155 events found without a reconstructed π^0. This number normalized to the integrated luminosity was subtracted from the event numbers at each energy point.

Figure 12d shows the gamma-gamma invariant mass distribution for all possible combinations of the photon pairs. The π^0 peak is very distinct. Figure 12b shows the gamma-gamma invariant mass distribution for the sample of events with all applied cuts. The resolution of the peak is in good agreement with expectations [9].

The ideal detector efficiency for this decay mode with these cuts is equal to 0.186$\pm$0.002, independently of the center of mass energy.

3.6 Selection of $\eta\gamma$ Events

This decay of the ϕ-meson with a branching ratio about 1% is searched for using the three pion decay of the η ($\eta \to \pi^+\pi^-\pi^0$). This mode is selected from a sample of events with two tracks of opposite charge. The selected tracks are assumed to be pions and should satisfy the following requirements:

1. The opening angle between two tracks is less than 2.5 radians to remove $K_S K_L$ events and azimuthal angular acollinearity is greater than 0.15 radians to remove K^+K^- events.

2. The vertex should be radially within 5 mm of the detector center and longitudinally within 10 cm.

3. The invariant mass of two pions is less than 520 MeV/c^2.

4. The missing mass squared of the two pions is greater than 100000 MeV^2/c^4 (missing mass is greater than 330 MeV/c^2).

The most energetic photon is assumed to be the photon from the primary $\phi \to \eta\gamma$ decay. Taking the η direction to be opposite to the photon candidate, calculating the η energy from the known beam energy, assuming the $\phi \to \eta\gamma$ decay, one can then calculate the missing mass in the rest system of the η. The resulting missing mass plot is shown in Figure 14.

The peak at the π^0 mass corresponds to $\eta \to \pi^+\pi^-\pi^0$ events, and an indication of an extra events near zero corresponds to $\eta \to \pi^+\pi^-\gamma$ events. The background under the π^0 mass peak was fit to a smooth function and subtracted from the peak to give the number of η decays in the main three pion channel.

Table V shows the number of selected events from the three pion decay for each energy point. The total number of events was found to be 279±21.

The efficiency for extracting the $\eta\gamma$ signal is 0.056±0.002 for the ideal detector; detailed efficiencies and corrections are shown in Table V.

3.7 Determination of the Center of Mass Energy

The energy of the machine was set roughly by the dipole magnet currents. A precise determination of the beam energy can be made using the measurement of the average momentum of the kaons in the K^+K^- final state at each energy point:

$$E_{beam} = \sqrt{p_K^2 + m_K^2} + \Delta_{dE/dx} + \Delta_{rad},$$

where $\Delta_{dE/dx}$ is the average ionization loss of the charged kaon and Δ_{rad} is the average radiative correction due to the emission of real gammas.

The average momentum resolution σ_{p_K} for the kaons with momenta around 110 MeV/c is about 5 MeV/c and determined mostly by the multiple scattering in DC. The statistical uncertainty in the beam energy is determined as

$$\sigma_{E_{beam}} = \frac{\sigma_{p_K} p_K}{E_{beam}\sqrt{N}},$$

where N is the number of found K^+K^- pairs. These uncertainties are very small and, depending on the number of events at each energy point, are in the range of 0.017 - 0.040 MeV.

It is known from the resonance depolarization study, that the beam energy in the collider with the fixed magnetic field varies with the average collider temperature as −0.032±0.010 MeV/degree and the day-night energy variations can be as high as 0.1-0.15 MeV. To take into account these and other possible variations, the measured average momenta for a group of runs with the same collider energy were plotted as a function of time and fit with a constant. This constant was further taken as an average momentum for a given beam energy and the obtained statistical error was increased by a scale factor S=$\sqrt{\chi^2}$, which increased statistical errors to 0.030-0.060 MeV.

The dE/dx correction together with Δ_{rad} were obtained by GEANT simulation of charged kaon events in the detector. The total calculated correction as a function of the measured average momentum is shown in Figure 15. The radiative corrections are about 100 keV and can be seen as a shoulder in this curve. The corrections are interpolated from this curve with an additional uncertainty of 0.015 MeV which is added quadratically to the statistical errors above.

The overall estimate for the systematic error in the absolute energy due to uncertainties in the material thickness (2%) and in the magnetic field measurement (0.1%) was done and gave a result of 0.092 MeV for one beam [23]. The estimated error in the slope of the calibration curve gives not more than 0.010 MeV systematic error in the ϕ-meson width.

Independent determination of the absolute beam energy from the energy calibration by the resonance depolarization method can be used to study systematic errors of the described procedure. Calibrations were performed at few energy points before and after data taking.

Using calibrated beam energies one can recalculate the value of the correction for measured kaon momentum. These values are plotted in Figure 15 and, assuming the same momentum dependence, a new calibration curve was

found. As a result, the calibration curve shifted down by 0.022 MeV. This corrected curve was used for the beam energy determination and the overall systematic error (doubled for the center of mass energy) in this determination was estimated to be 0.024 MeV.

The results of the energy determination, together with the luminosity and other relevant quantities, are given in Table I. Only statistical errors are presented.

3.8 Radiative Corrections and Cross Section Calculation

The following formula was used for calculation of the cross section at each energy point for each channel:

$$\sigma = \frac{N}{L \cdot \epsilon_{ideal} \cdot \epsilon_{rec} \cdot \epsilon_{trig} \cdot (1 + \delta_{rad})}.$$

Determination of the integrated luminosity and efficiencies was described in previous sections.

The high statistical accuracy achieved in this experiment and even higher data samples expected to be collected in future runs require knowledge of the radiative corrections with an accuracy better than 0.5%, for all investigated channels of e^+e^- annihilation. At this level of accuracy it is necessary to take into account the influence of the radiative effects on the kinematics of the final particles. This is possible if Monte Carlo simulation is based on the differential cross section of the process over all final particles, including emitted photons.

Radiative corrections for the cross sections of the main channels of e^+e^- annihilation into hadrons and leptons were calculated according to [16, 17, 18]. For leptonic channels ($e^+e^-, \mu^+\mu^-$) the radiation of both initial and final state particles was taken into account. The theoretical uncertainty of the cross sections of the $\mu^+\mu^-$ and hadronic channels corrected for radiative effects varied from 0.2% to 0.5% depending on the reaction channel. For the Bhabha scattering the results of Ref. [18] were used. The theoretical uncertainty in that work is about 1%, which is more than the required 0.5% stipulated above. We expect to improve the accuracy in the calculation of this cross section by taking into account the contribution of the next order diagrams [19]. More details can be found elsewhere [20].

The radiative corrections used for each of the main decay modes of the ϕ, are shown in Tables II-V together with the resulting cross sections. The

uncertainties of the cross sections include both statistical and systematic errors which were introduced for each point separately. Also included were errors caused by the influence of the uncertainty of energy determination on the radiative corrections and on the cross sections themselves.

3.9 Fits to Data

The experimental cross sections measured for each decay mode (see Tables I-V) were used to obtain ϕ meson parameters by fitting experimental points to its resonance curves.

The cross section of the kaon production can be written as:

$$\sigma(s) = \frac{\pi \cdot \alpha^2}{12} \cdot \frac{P_{2K}(s)}{s^{5/2}} \cdot |F_k(s)|^2,$$

where P_{2K}(s) is a phase space for two kaons, and in the framework of the vector dominance model (VDM) the kaon formfactor can be written as:

$$F_{K^\pm} = \left(\frac{g_{\rho\gamma}g_{\rho K\bar{K}}}{\Delta\rho} + \frac{g_{\omega\gamma}g_{\omega K\bar{K}}}{\Delta\omega} + \frac{g_{\phi\gamma}g_{\phi K\bar{K}}}{\Delta\phi}\right) \cdot \sqrt{C}(s)$$

and

$$F_{K^0} = -\frac{g_{\rho\gamma}g_{\rho K\bar{K}}}{\Delta\rho} + \frac{g_{\omega\gamma}g_{\omega K\bar{K}}}{\Delta\omega} + \frac{g_{\phi\gamma}g_{\phi K\bar{K}}}{\Delta\phi}.$$

The propagators of the vector mesons are $\Delta v = s - m_v^2 + i\sqrt{s}\Gamma_v(s)$, with the energy dependence of the width as in [21]

$$\Gamma_\rho(s) = \Gamma_\rho \cdot \frac{m_\rho^2 P_{2\pi}(s)}{s P_{2\pi}(m_\rho^2)},$$

$$\Gamma_\omega(s) = \Gamma_\omega \cdot \left(B_{3\pi}\frac{s^{3/2}P_{3\pi}(s)}{m_\omega^3 P_{3\pi}(m_\omega^2)} + B_{2\pi}\frac{m_\omega^2 P_{2\pi}(s)}{s P_{2\pi}(m_\omega^2)} + B_{\pi^0\gamma}\frac{m_\omega^2 P_{\pi^0\gamma}(s)}{s P_{\pi^0\gamma}(m_\omega^2)}\right),$$

$$\Gamma_\phi(s) = \Gamma_\phi \cdot \left(B_{K^+K^-}\frac{m_\phi^2 P_{2K^\pm}(s)}{s P_{2K^\pm}(m_\phi^2)} + B_{K_SK_L}\frac{m_\phi^2 P_{2K^0}(s)}{s P_{2K^0}(m_\phi^2)} + \right.$$

$$\left. + B_{3\pi}\frac{s^{3/2}P_{3\pi}(s)}{m_\phi^3 P_{3\pi}(m_\phi^2)} + B_{\eta\gamma}\frac{m_\phi^2 P_{\eta\gamma}(s)}{s P_{\eta\gamma}(m_\phi^2)}\right),$$

where B_f are the branching ratios of the major decay modes of ϕ, ω and ρ and P_f(s) are phase space factors. For two-particle decays the phase space factor is determined by a momentum of final particle as $P_f(s)=(s/4-m_f^2)^{3/2}$, for the

radiative decay into $\eta\gamma$ $P_{\eta\gamma}(s) = (\sqrt{s}/2(1 - m_\eta^2/s))^3$ and for the three pion final state it is a function obtained by the numerical calculation assuming the $\phi \to \rho\pi \to 3\pi$ model [21]. C(s) is the factor describing the interaction of the charged kaons in the final state which is absent for the neutral kaon mode.

Using the experimental values of the electronic widths [24] for the coupling constants $g_{v\gamma}$ and assuming SU(3) relations with ideal mixing

$$g_{\rho K\bar{K}} = g_{\omega K\bar{K}} = \frac{1}{\sqrt{2}} g_{\phi K\bar{K}},$$

the kaon formfactors may be expressed like

$$F_{K^\pm} = g_{\phi\gamma} g_{\phi K\bar{K}} \cdot \sqrt{C}(s) \cdot (\Delta\rho^{-1} + \frac{1}{3}\Delta\omega^{-1} + \Delta\phi^{-1}),$$

$$F_{K^0} = g_{\phi\gamma} g_{\phi K\bar{K}} \cdot (-\Delta\rho^{-1} + \frac{1}{3}\Delta\omega^{-1} + \Delta\phi^{-1}).$$

In the approximation of soft photon exchange the factor $C(s)$ may be written as C(s)=Z(1+$Z^2/4\pi^2$)/(1-e^{-Z}), Z=$2\pi m_K/p_K$ [22] and increases the cross section by about 5% (usually referred to as Coulomb factor). In our kaon momentum range and the present experimental statistics the energy dependence is negligible and the Coulomb factor may be included into the coupling constant for charged kaons, making it different from one for neutral kaons during the fits. It should be emphasized once again that the particular expression for the Coulomb factor used above is based on the assumption of the exchange by soft photons only. A more sophisticated approach could in principle further change the relation between charged and neutral kaon constants.

The cross section may be rewritten in terms of σ^0 - the cross section in the peak of the resonance for the selected channel:

$$\sigma_K(s) = \sigma_K^0 \cdot \frac{P_{2K}(s)}{P_{2K}(m_\phi^2)} \cdot \frac{m_\phi^7 \Gamma_\phi^2}{s^{5/2}} \cdot |\pm\Delta\rho^{-1} + \frac{1}{3}\Delta\omega^{-1} + \Delta\phi^{-1}|^2.$$

For the decays into $\pi^+\pi^-\pi^0$ and $\eta\gamma$ in the frame of the VDM the cross section may be written in the same way as:

$$\sigma_{3\pi,\eta\gamma}(s) = \frac{P_{3\pi,\eta\gamma}(s)}{s^{3/2}} \cdot |A_\omega + A_\phi e^{i\delta_\phi} + A_{bkg}|^2,$$

$$A_v = \frac{m_v^{5/2}\Gamma_v^0\sqrt{\sigma^0/P(m_v^2)}}{\Delta v},$$

$$A_{bkg} = m_\phi^{3/2}\sqrt{\sigma_{bkg}/P(m_\phi^2)},$$

where σ_{bkg} and δ_ϕ are a nonresonant background and a relative phase of ϕ-ω mixing respectively. Only the interference with ω is taken into account as a dominant one. The peak cross sections for ω were calculated from the PDG values of the width and branching ratio [24]. The nonresonant background cross section σ_{bkg} was determined only for the three pion channel.

All four processes were fitted together. The peak cross sections σ^0 for each mode, mass and width of ϕ, nonresonant background and the relative phase for the three pion decay mode were parameters in the fit. As a result of the fit σ_{bkg}=0.56±0.46 nb and was further fixed to zero. The following results were obtained:

$m_\phi = 1019.380 \pm 0.034 \pm 0.048$ MeV ,
$\Gamma_\phi = 4.409 \pm 0.086 \pm 0.020$ MeV,
$\sigma(\phi \to K^+K^-) = 1993 \pm 65 \pm 82$ nb,
$\sigma(\phi \to K_S K_L) = 1360 \pm 25 \pm 49$ nb,
$\sigma(\phi \to 3\pi) = 656 \pm 24 \pm 30$ nb ,
$\sigma(\phi \to \eta\gamma) = 47.9 \pm 3.5 \pm 3.2$ nb,
$\delta_\phi = (147 \pm 16)^o$.

The first error represents the statistical uncertainty which includes all systematic uncertainties for each individual energy point. The second one is the overall systematic uncertainty, which, for the cross sections, comes from the uncertainties in the trigger efficiencies (see Table VI), simulated ideal efficiencies (see Sections 3.3-3.6) and from the uncertainty in the luminosity measurement (3%). The relative phase is in good agreement with the most precise measurement presented in [4] $\delta_\phi = (155 \pm 15)^o$.

The excitation curves of the ϕ in different modes, together with the experimental points, are shown in Figure 16.

In this experiment all the major decay modes were simultaneously measured in one detector and therefore the branching ratios can be obtained as ratios of integrals over excitation curves independently of the width of the ϕ and the normalization uncertainties related to the luminosity measurements. In this case instead of σ^0_{peak} for each mode $\sigma^0_{peak} \cdot \Gamma_\phi$ was a free fit parameter allowing to remove correlations in the errors. The following results were obtained:

B($\phi \to K^+K^-$) = 49.1 ± 1.2 % ,
B($\phi \to K_S K_L$) = 33.5 ± 1.0 % ,

$B(\phi \to 3\pi) = 16.2 \pm 0.8$ % ,
$B(\phi \to \eta\gamma) = 1.18 \pm 0.11$ % .

The errors given here correspond to the statistical and systematic uncertainties added in quadrature. The branching ratios have not been corrected for the known 0.2% of decays to other modes, since this correction is much less than our errors. The electron width and branching ratio to e^+e^- of the ϕ can also be calculated independently as $\Gamma_{ee} = m_\phi^2/12\pi \cdot \sum \sigma_i^0 \Gamma_\phi$, assuming $\sum B_i = 1$ and are found to be

$\Gamma_{ee} = 1.27 \pm 0.05$ keV,
$B(\phi \to ee) = (2.87 \pm 0.09) \times 10^{-4}$.

All obtained results are consistent with the Particle Data Group values [24]. There is a small (approximately 2 σ) difference in the Γ_{ee} and $B(\phi \to ee)$ - the PDG [24] gives 1.37±0.05 keV and $(3.09 \pm 0.07) \times 10^{-4}$. Note that our value of the electron width is between the current values of the muon and electron widths quoted by the PDG [24] $B(\phi \to \mu\mu) = (2.48 \pm 0.34) \times 10^{-4}$.

The final values for the mass and width from all the channels are:

$m_\phi = 1019.38 \pm 0.06$ MeV ,
$\Gamma_\phi = 4.41 \pm 0.09$ MeV,

to be compared with the best ones from previous e^+e^- collider experiments: $m_\phi = 1019.54 \pm 0.12$ MeV, Γ_ϕ=4.36±0.29 MeV [3] and to the Particle Data Group average of $m_\phi = 1019.411 \pm 0.008$ MeV, $\Gamma_\phi = 4.43 \pm 0.06$ MeV.

4 Conclusions

In conclusion note that the measurement of the parameters of the ϕ and its four major decay modes demonstrates the ability of the detector for precise measurements. For the first time the major parameters of the ϕ have been measured in one experiment. Analysis of an event sample in total 5 times the data presented here is in progress and will allow new results on rare decay modes of the ϕ, including channels of interest for the design of ϕ factory detectors as well as more complete studies of systematic errors[15]. The connections between the CMD-2 research program and the future Φ factory projects with luminosity $(1-3) \times 10^{33} cm^{-2} s^{-1}$ in Novosibirsk [25] and at Frascati [26, 27]. have been described elsewhere [28, 29, 30, 31].

Acknowledgements. The authors would like to thank M.B. James, R. R. Rose, U.Y. Washington, and J.H. Herald for help with the production of simulated data and the technical personal of VEPP-2M for the machine and detector support during experimental runs. We also would like to thank N.N.Achasov, G.N.Shestakov, V.N.Ivanchenko, V.M.Fadin for usefull discussions.

The present work was supported in part by grants from the Russian government, and from the government of the United States through grants from the Department of Energy and the National Science Foundation and also from the grant RPT000 of the International Science Foundation.

References

[1] V. V. Anashin et al., Preprint INP 84-114, Novosibirsk,1984.

[2] L.M. Barkov et al., Nucl. Phys. **B256** (1985) 365.

[3] A.D. Bukin et al., Sov. Journal of Nucl. Phys. **27** (1978) 516.

[4] S.I.Dolinsky et al., Phys. Reports **202** (1991) 99.

[5] E.V. Anashkin et al., ICFA Instrumentation Bulletin 5 (1988), and G.A. Aksenov et al., Preprint INP 85-118, Novosibirsk, 1985.

[6] V.M. Aulchenko et al., Nucl. Instr. and Methods **A252** (1986) 299.

[7] E.V.Anashkin et al., Nucl. Instr. and Methods **A323** (1992) 178.

[8] L.M.Barkov et al., Proc. of 5th International Conference on Instrumentation for Colliding Beam Physics, Novosibirsk, March, 1990, p.480.

[9] B.A. Shwartz et al., Proc. of 5th International Conference on Instrumentation for Colliding Beam Physics., Novosibirsk, March, 1990, p.318.

[10] V.M. Aulchenko et al., Nucl. Instr. and Methods **A265** (1988) 137.

[11] V.M. Aulchenko et al., Preprint INP 88-43, Novosibirsk, 1988.

[12] G.A. Aksenov et al., Proc. of the International Conference on Computing in High Energy Physics, Annecy, France, 1992, p.783.

[13] T.A.Purlatz, CMD2SIM User's Guide, CMD2 internal note, Novosibirsk, September 1993.

[14] R.R.Akhmetshin et al., Preprint BudkerINP, to be published, Novosibirsk, 1995.

[15] E.P.Solodov, Florida Intersections Conference, USA, May 1994. E.P.Solodov et al. Proceedings of the Second Workshop on Physics and Detectors for DAΦNE, Frascati, April, 1995.

[16] E.A.Kuraev and V.S.Fadin, Sov. Journal of Nucl. Phys. **41** (1985) 466.
E.A.Kuraev and V.S.Fadin, Preprint INP 86-114, Novosibirsk, 1986.

[17] E.A.Kuraev and S.N.Panov, Preprint INP 91-26, Novosibirsk, 1991.

[18] F.A.Berends and R.Kleiss, Nucl. Phys. **B228** (1983) 537.

[19] V.A.Astakhov and E.A.Kuraev, Preprint INP,to be published, Novosibirsk, 1995.

[20] S.I.Eidelman et al., Preprint INP 95-34, Novosibirsk, 1995. G.V.Fedotovich et al., Proceedings of the Second Workshop on Physics and Detectors for DAΦNE, Frascati, April, 1995.

[21] N.N.Achasov et al., Sov. Journal of Nucl. Phys. **23** (1976) 320.

[22] V.S.Fadin et al., Sov. Journal of Nucl. Phys. **53** (1991) 1118.

[23] E. Popkov, CMD-2 internal note.

[24] L.Montanet et al., Phys. Rev. **D50** (1994) 1173.

[25] A. Skrinsky, Proceedings of the Workshop on Physics and Detectors for DAΦNE, Frascati, April, 1991, p.67.

[26] F. Vignola, Proceedings of the Workshop on Physics and Detectors for DAΦNE, Frascati, April, 1991, p.11.

[27] P. Franzini, Proceedings of the XXVI International Conference on High Energy Physics, August 6-12, 1992, Dallas, Texas, p.1885.

[28] S. Eidelman, E. Solodov, and J. Thompson, Nucl. Phys. B (Proceedings Supplement) **24A** (1991) 174.

[29] R. Demina, V. Savinov, and J.A. Thompson, Proceedings of the Workshop on Physics and Detectors for DAΦNE, Frascati, April, 1991, p.515.

[30] S. Eidelman, J.A. Thompson, and C.H. Yang, Proceedings of the Workshop on Physics and Detectors for DAΦNE, Frascati, April, 1991, p.437.

[31] B.I. Khazin et al., Proceedings of the XXVI International Conference on High Energy Physics, August 6-12, 1992, Dallas, Texas, p. 1876.

Table I: Energy, Number of collinear events, Calculated Cross Section, Reconstruction efficiency and Luminosity

n.n	$E_{c.m.}$±dE,MeV	N_{coll}±dN	σ_{coll},nb	ϵ_{rec}±dϵ	L±dLnb^{-1}
1	993.956±0.600	8440± 96	570	0.998±0.002	15.41±0.21
2	1008.624±0.402	7612± 91	544	0.912±0.007	15.97±0.22
3	1013.882±0.182	5911± 81	536	0.892±0.009	12.87±0.21
4	1016.726±0.090	4627± 72	532	0.894±0.010	10.13±0.19
5	1017.264±0.096	5066± 80	531	0.833±0.007	11.92±0.21
6	1017.654±0.094	6498± 83	531	0.848±0.006	15.02±0.21
7	1017.934±0.082	6704± 94	531	0.848±0.006	15.50±0.24
8	1017.982±0.066	21247±148	530	0.969±0.002	43.07±0.31
9	1018.322±0.066	13373±123	530	0.783±0.004	33.55±0.34
10	1018.806±0.074	4945± 88	530	0.783±0.004	12.40±0.22
11	1019.070±0.070	10073±128	530	0.833±0.007	25.27±0.34
12	1019.468±0.104	2097± 49	531	0.833±0.007	4.94±0.12
13	1019.636±0.094	1637± 55	532	0.783±0.004	4.09±0.13
14	1021.762±0.084	5814± 98	534	0.783±0.004	14.47±0.25
15	1022.072±0.096	7002± 89	534	0.800±0.005	17.06±0.23
16	1027.996±0.124	15907±140	531	0.807±0.003	39.16±0.37

Table II: Number of K^+K^- events, Efficiencies, Radiative Corrections and Experimental Cross Sections

n.n	N±dN_{K+K-}	ϵ_{ideal}	ϵ_{rec}±dϵ_{rec}	radcorr	σ±dσ,nb
2	10±10	0.0229	0.855±0.034	-0.230	50± 50
3	31± 7	0.0218	0.791±0.031	-0.240	222± 54
4	76±11	0.0210	0.813±0.022	-0.255	713±114
5	107±14	0.0209	0.803±0.016	-0.255	897±134
6	188±18	0.0208	0.803±0.012	-0.260	1224±135
7	193±18	0.0205	0.803±0.012	-0.260	1236±137
8	768±33	0.0205	0.962±0.006	-0.260	1477± 87
9	488±32	0.0205	0.630±0.005	-0.265	1844±143
10	179±20	0.0205	0.630±0.005	-0.270	1852±219
11	454±28	0.0204	0.630±0.005	-0.270	2317±166
12	106±13	0.0203	0.803±0.006	-0.260	2152±272
13	63±11	0.0203	0.630±0.005	-0.250	1939±347
14	133±16	0.0197	0.630±0.005	-0.090	973±126
15	129±17	0.0197	0.685±0.014	-0.070	719±104
16	90±13	0.0180	0.754±0.015	0.245	161± 25

Table III: Number of K_SK_L events, Efficiencies, Radiative Corrections and Experimental Cross Sections

n.n	N±dN_{KsKl}	ϵ_{ideal}	ϵ_{rec}± dϵ_{rec}	radcorr	σ±dσ,nb
2	64±15	0.372	0.862±0.040	-0.235	18± 5
3	379±23	0.365	0.840±0.028	-0.235	137±14
4	1122±35	0.362	0.889±0.020	-0.250	504±35
5	1759±47	0.361	0.822±0.011	-0.260	739±49
6	2562±56	0.360	0.847±0.007	-0.260	831±47
7	2958±58	0.360	0.847±0.018	-0.265	937±53
8	9858±95	0.360	0.966±0.003	-0.265	985±40
9	6671±85	0.359	0.747±0.005	-0.270	1118±46
10	2817±64	0.359	0.747±0.005	-0.270	1277±52
11	5856±93	0.359	0.747±0.005	-0.270	1303±46
12	1379±41	0.358	0.822±0.011	-0.260	1411±62
13	996±36	0.358	0.747±0.005	-0.250	1334±68
14	2125±65	0.355	0.747±0.005	-0.100	669±36
15	2280±51	0.354	0.770±0.009	-0.080	579±30
16	1388±51	0.348	0.789±0.009	0.250	138±14

Table IV: Three Pion events, Efficiencies, Radiative Corrections and Experimental Cross Sections

n.n	N±d$N_{3\pi}$	ϵ_{ideal}	ϵ_{rec}±dϵ_{rec}	radcorr	σ±dσ,nb
1	155±15	0.1856	0.980±0.020	-0.075	31± 9
2	188±14	0.1856	0.855±0.054	-0.160	54±12
3	278±17	0.1856	0.791±0.031	-0.210	158±18
4	439±21	0.1856	0.813±0.022	-0.240	373±29
5	597±26	0.1856	0.803±0.016	-0.245	447±32
6	786±30	0.1856	0.803±0.012	-0.250	473±31
7	931±30	0.1856	0.803±0.012	-0.255	554±32
8	3025±53	0.1856	0.962±0.006	-0.250	545±22
9	1746±46	0.1856	0.663±0.005	-0.250	570±30
10	708±30	0.1856	0.663±0.005	-0.250	631±39
11	1506±46	0.1856	0.663±0.005	-0.250	662±29
12	314±20	0.1856	0.803±0.006	-0.235	575±45
13	239±16	0.1856	0.663±0.005	-0.220	621±53
14	471±27	0.1856	0.663±0.005	-0.025	252±24
15	499±24	0.1856	0.765±0.014	0.005	187±18
16	405±22	0.1856	0.794±0.015	0.760	21± 5

Table V: Number of $\eta\gamma$ events, Efficiencies, Radiative Corrections and Experimental Cross Sections

n.n	N±d$N_{\eta\gamma}$	ϵ_{ideal}	ϵ_{rec}±dϵ_{rec}	radcorr	σ±dσ,nb
2	2.7± 1.6	0.0562	0.855±0.034	-0.200	4.9± 2.9
3	2.0± 1.0	0.0562	0.791±0.031	-0.220	5.0± 2.6
4	10.0± 3.5	0.0562	0.813±0.022	-0.240	32.0±11.3
5	7.0± 2.0	0.0562	0.803±0.016	-0.245	19.4± 5.8
6	16.7± 4.2	0.0562	0.803±0.012	-0.250	36.9± 9.5
7	12.6± 3.7	0.0562	0.803±0.012	-0.250	27.0± 8.1
8	72.0±10.0	0.0562	0.962±0.006	-0.250	46.4± 6.6
9	29.7± 6.5	0.0562	0.706±0.009	-0.260	33.9± 7.6
10	14.9± 4.5	0.0562	0.706±0.009	-0.260	46.0±14.0
11	36.8± 6.7	0.0562	0.706±0.009	-0.265	56.2±10.4
12	8.9± 3.0	0.0562	0.803±0.016	-0.255	60.3±20.4
13	4.0± 2.0	0.0562	0.706±0.009	-0.235	36.2±18.2
14	13.6± 4.0	0.0562	0.706±0.009	-0.070	28.3± 8.4
15	13.7± 4.0	0.0562	0.865±0.014	-0.050	24.4± 7.2
16	6.2± 2.8	0.0562	0.754±0.015	0.420	2.9± 1.3

Table VI: Trigger efficiencies, extracted from the dedicated runs

Trigger type	ϵ_{trig} for coll. events	ϵ_{trig} for K+K- events	ϵ_{trig} for K_sK_L events	ϵ_{trig} for 3π events
CsI	1.000	0.924±0.013	0.964±0.011	0.980±0.010
TF	0.961±0.010	0.912±0.016	0.961±0.008	0.923±0.034
CsI*TF	0.961±0.010	0.843±0.019	0.926±0.014	0.904±0.037
	1.000	0.877±0.021	0.964±0.018	0.942±0.040

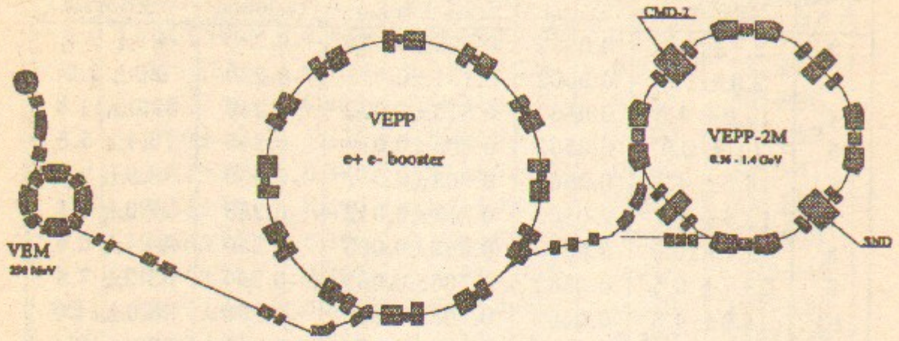

Figure 1. The layout of the VEPP-2M collider at the Budker Institute of Nuclear Physics in Novosibirsk.

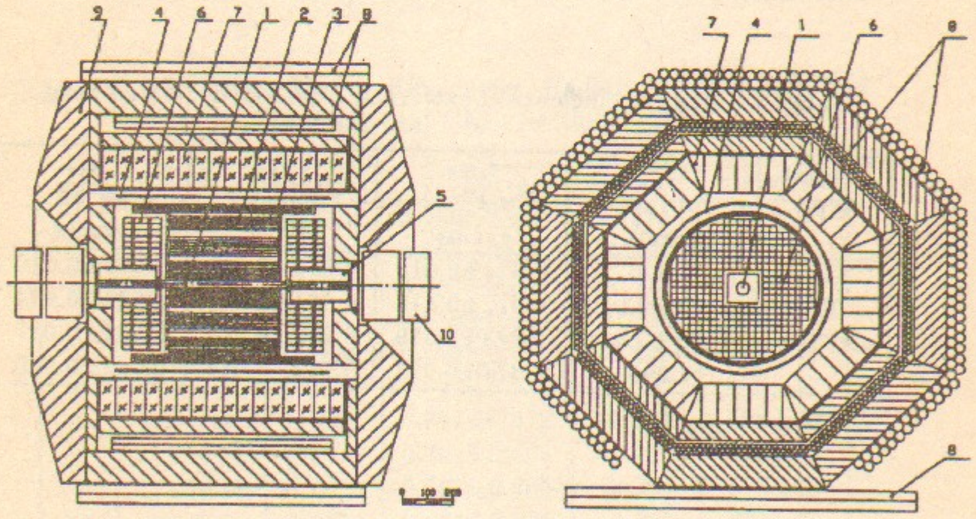

Figure 2. Horizontal and vertical cross sections of the CMD-2 detector. 1 – vacuum chamber; 2 – drift chamber; 3 – Z-chamber; 4 – superconducting solenoid; 5 – compensating solenoid; 6 – storage ring lenses; 7 – calorimeter; 8 – muon range system; 9 – magnet yoke

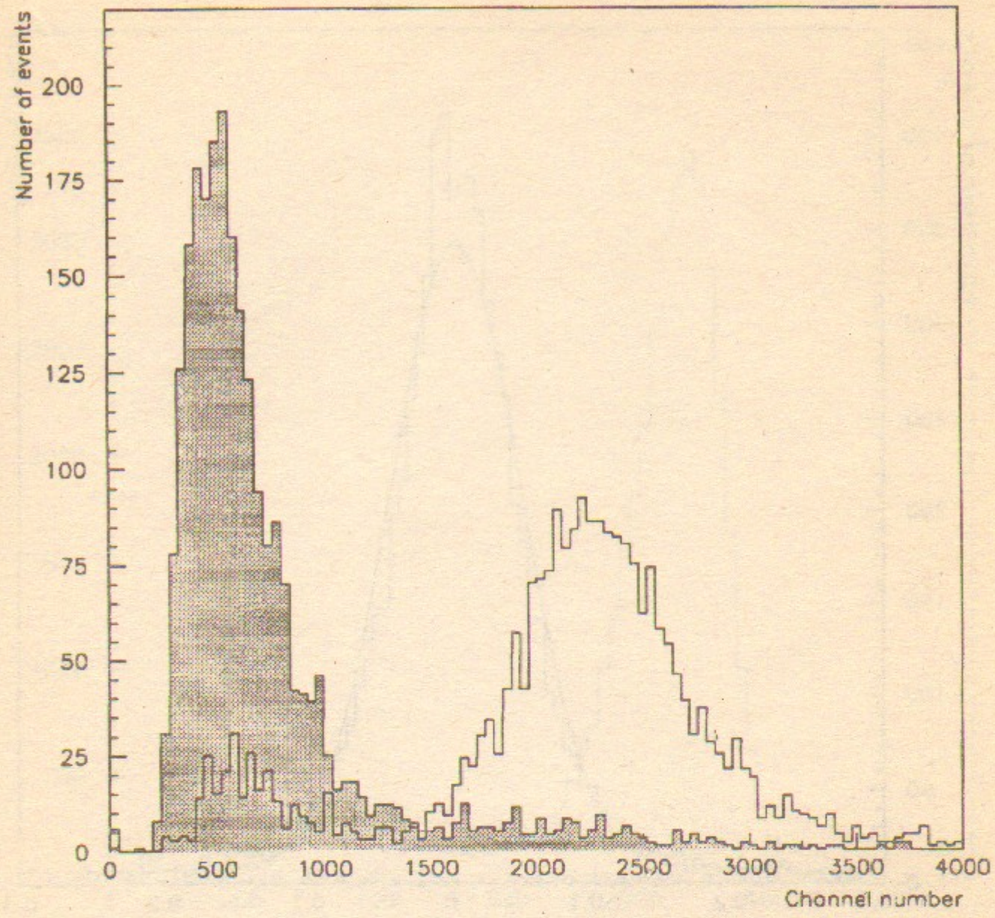

Figure 3. dE/dx in the drift chamber for the collinear events. Minimun ionizing particles are shown shaded.

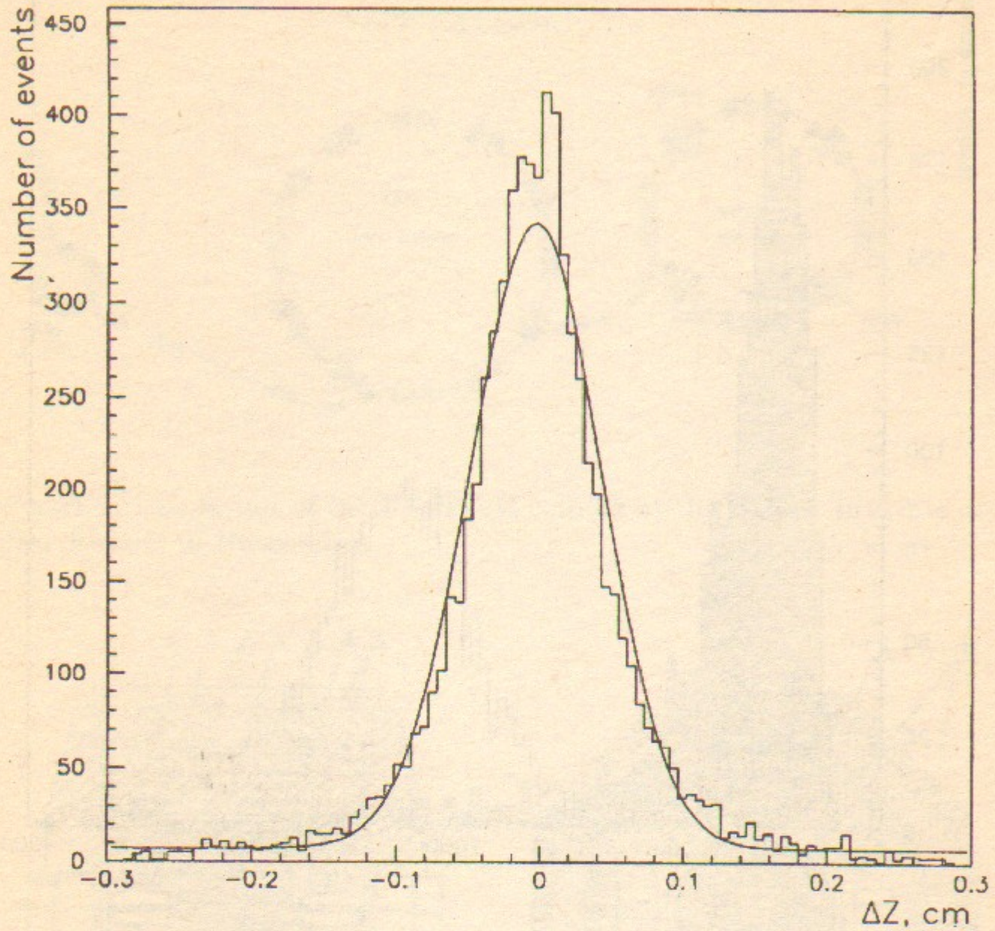

Figure 4. Z-chamber resolution along the Z-coordinate, extracted from collinear events.

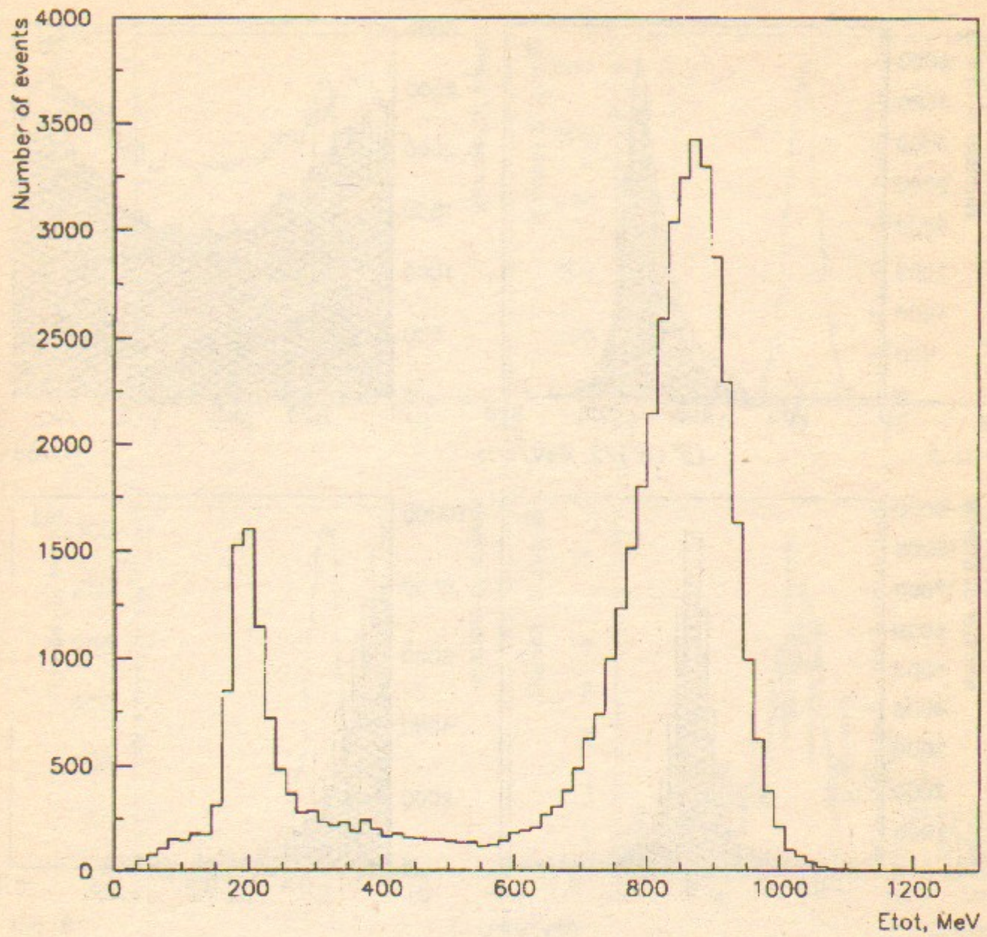

Figure 5. Energy deposition in CsI calorimeter for the events with two reconstructed tracks in the drift chamber.

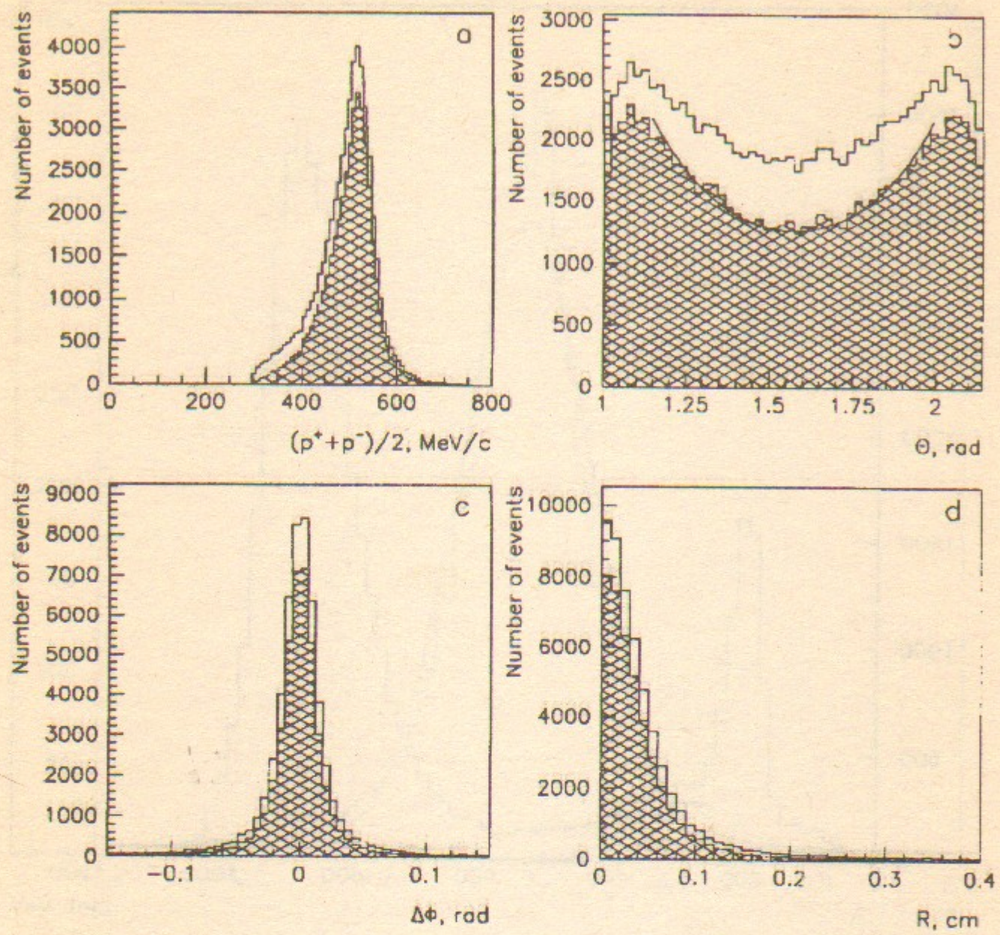

Figure 6. The distributions used in selection of the collinear events. *a*) The average momentum of the collinear events.The resolution is about 6%; *b*) polar angle distribution of the collinear events; *c*) $\Delta\phi$, in radians. The resolution is about 1 mrad.; *d*) The radial distance of the two-track vertex from the nominal collision point. The striped histograms present distributions of only Bhabha events, selected by energy deposition in the calorimeter.

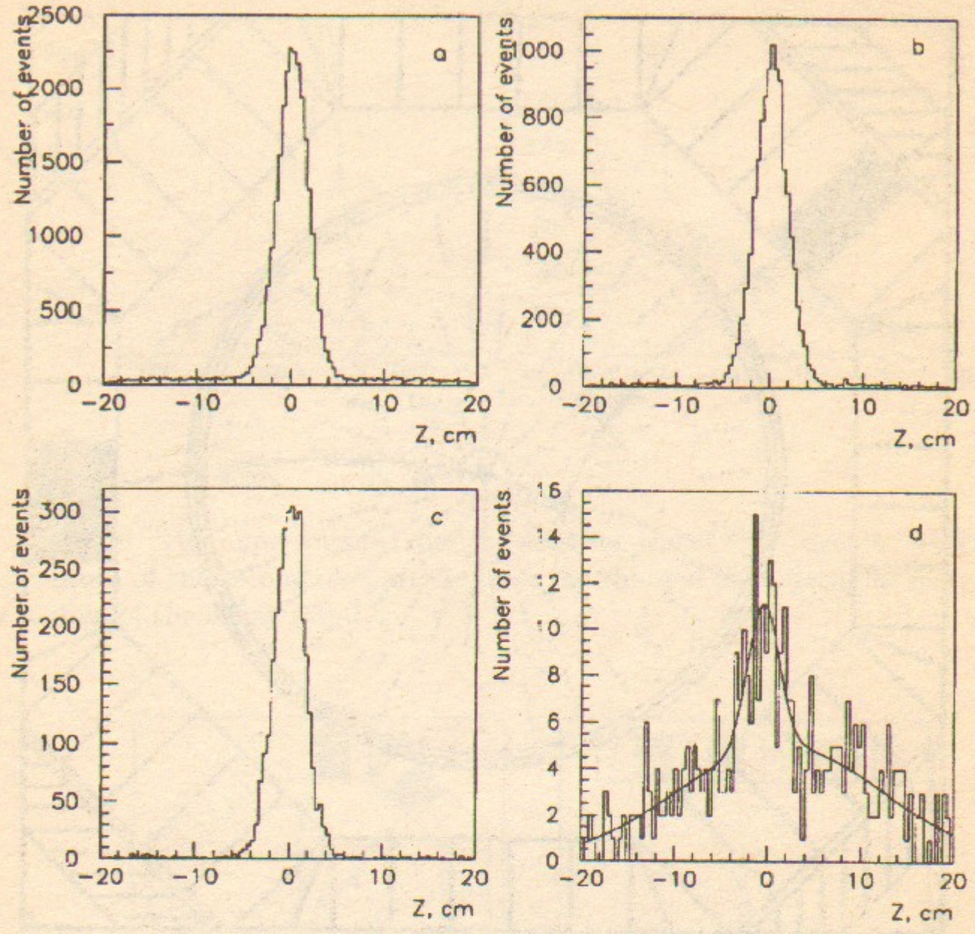

Figure 7. Z-vertex distribution for different types of event. *a*) collinear events; *b*) $K_S K_L$ events; *c*) three pion events; *d*) $K_S K_L$ events at $E_{beam} =$ 504.4 MeV.

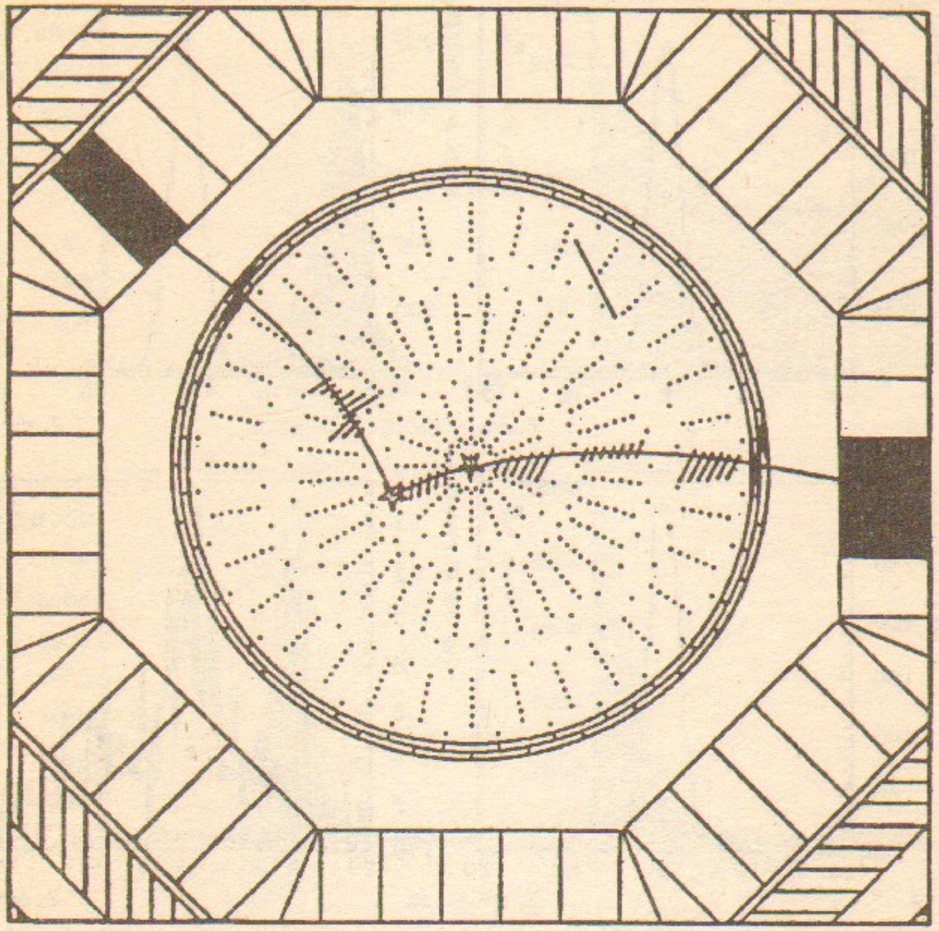

Figure 8. An example of an event with two charged kaons with one kaon decaying in flight.

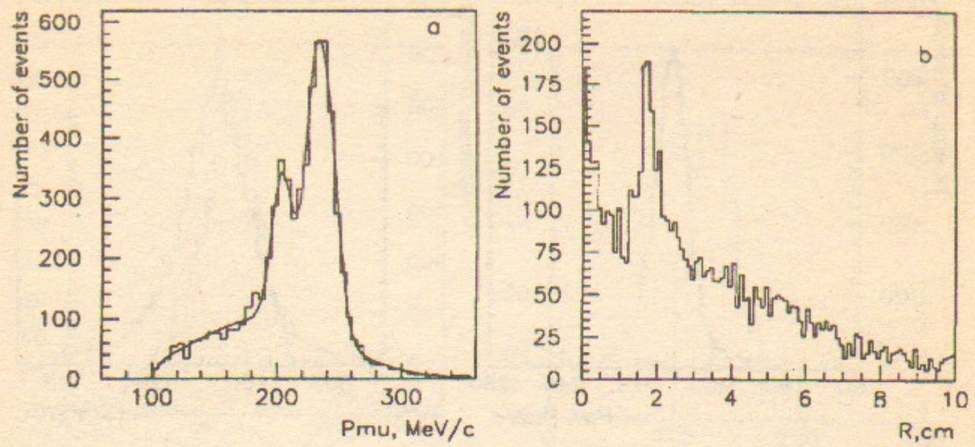

Figure 9. The experimental distributions for the K^+K^- events. *a*) The momentum of the secondary particle from the charged kaon decay at rest; *b*) the radius of the decay point.

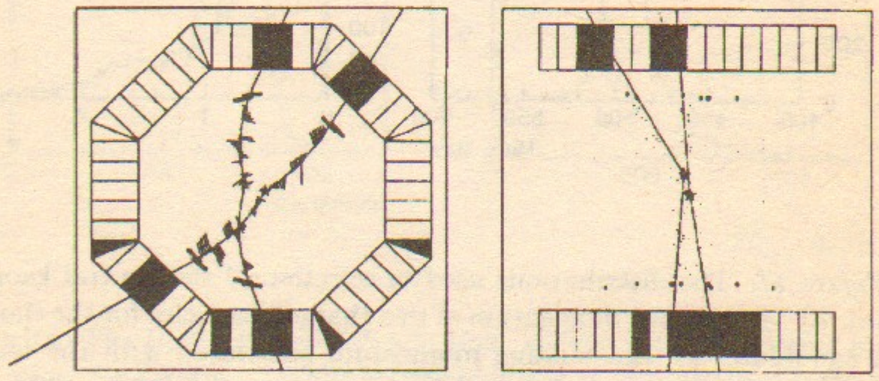

Figure 10. A picture of a neutral kaon event in which both kaons decay to two charged particles.

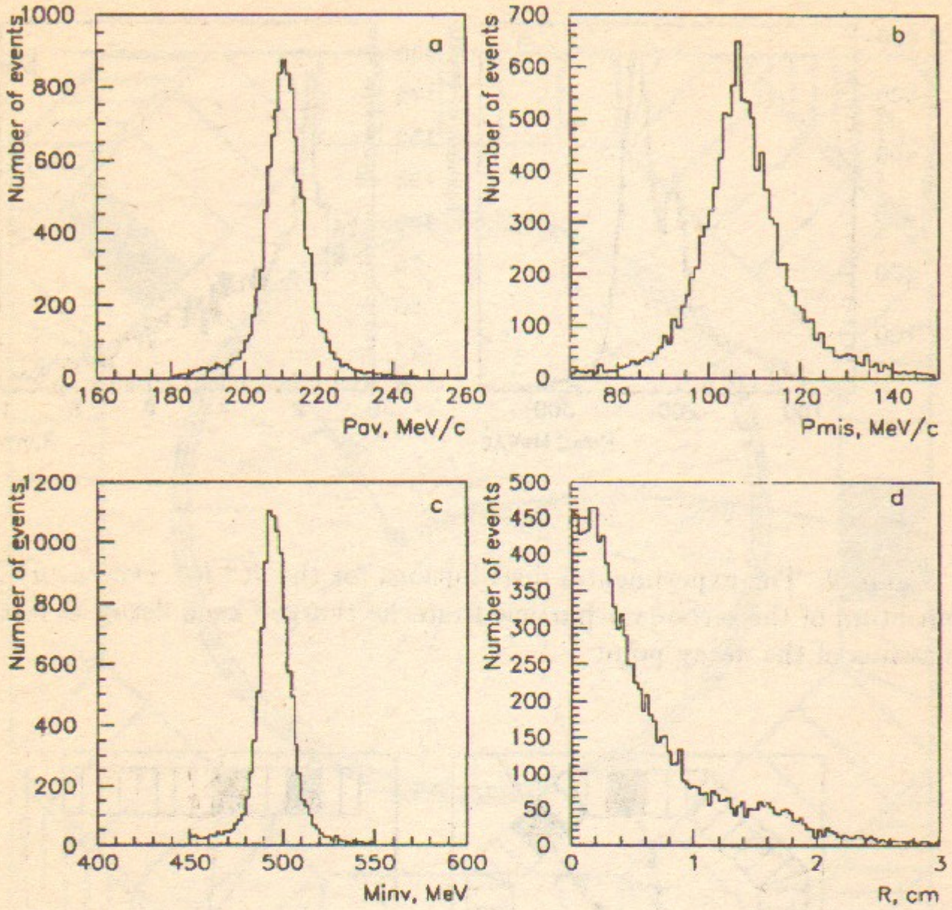

Figure 11. The distributions used in selection of the neutral kaon decay modes. *a*) The average momentum of two charged particles for the short-lived kaon candidate; *b*) The missing momentum associated with the long-lived kaon; *c*) the invariant mass of the short-lived kaon candidate; *d*) the radial vertex distance of the short-lived kaon decay.

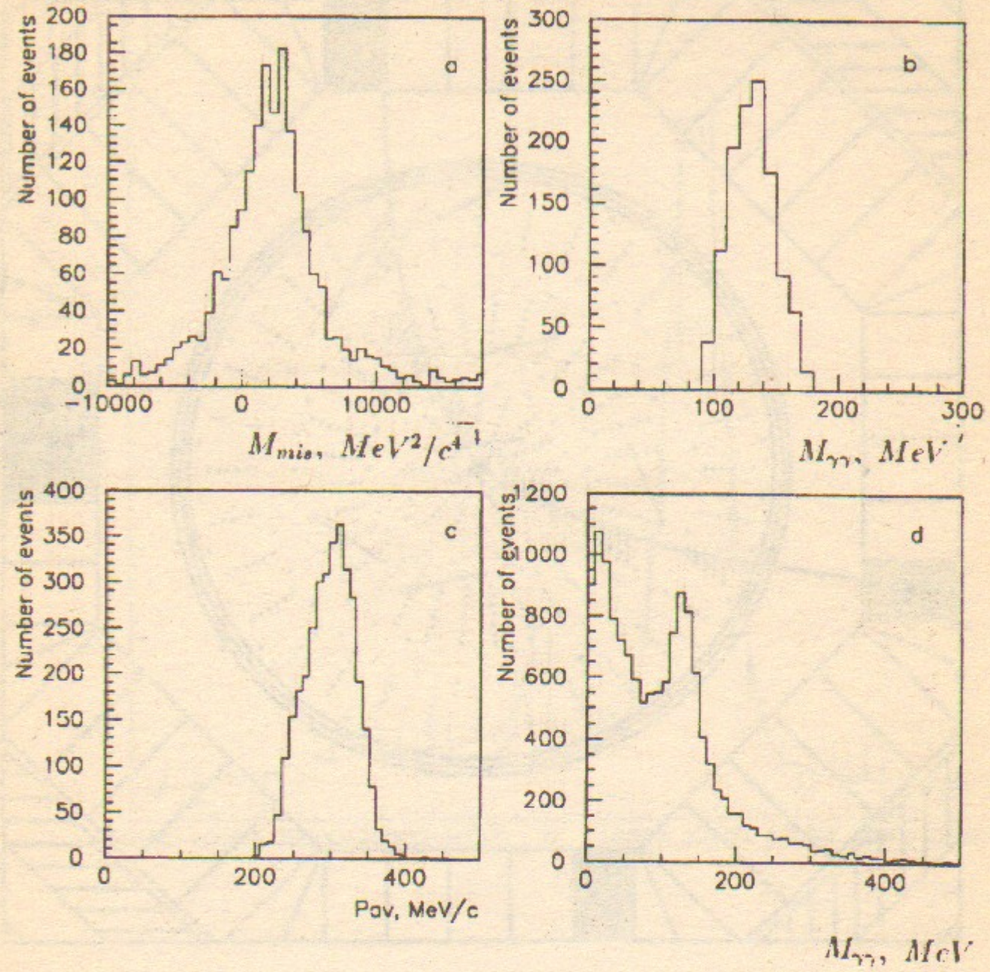

Figure 12. The three pion events selection. *a*) The squared missing mass for three pion candidates. *b*) The invariant mass of two photons from the CsI calorimeter for events with two selected charged tracks. *c*) The average momentum of the two charged particles for three pion candidates. *d*) The invariant mass for each pair of photons from the CsI calorimeter for the events with any number of photons.

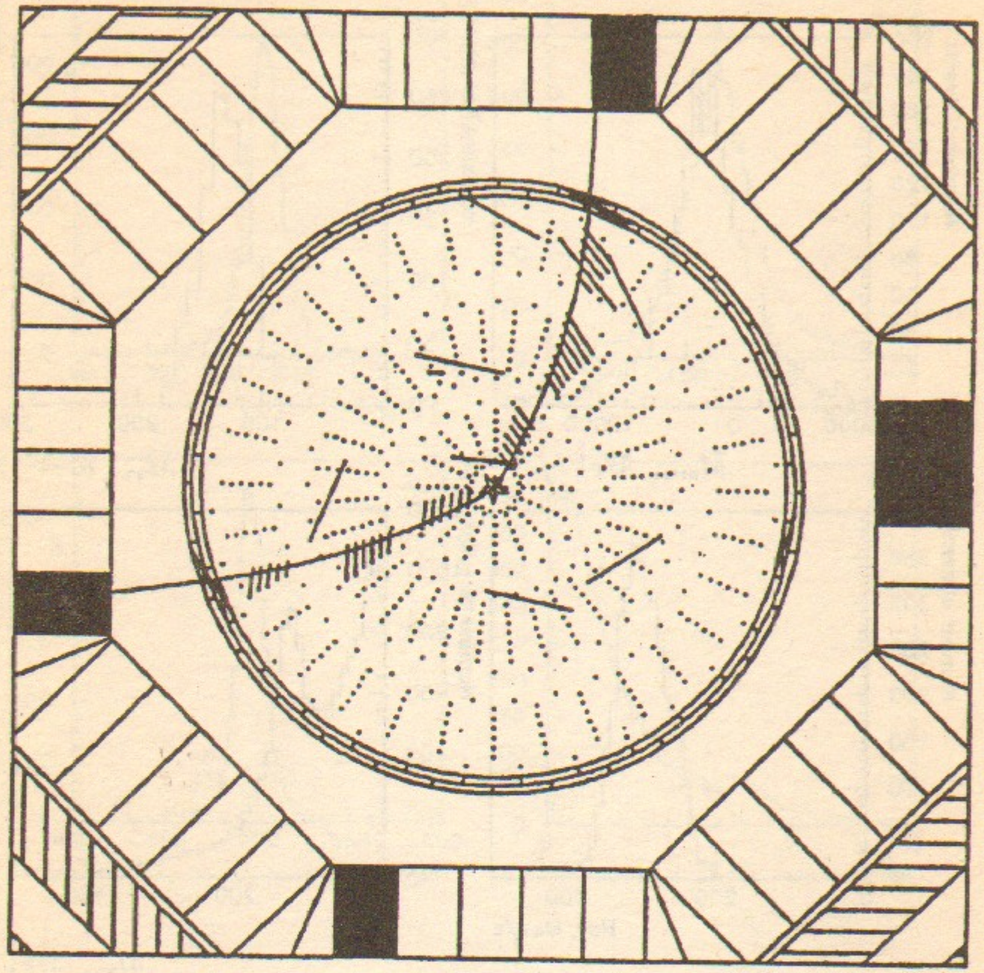

Figure 13. The three pion event display.

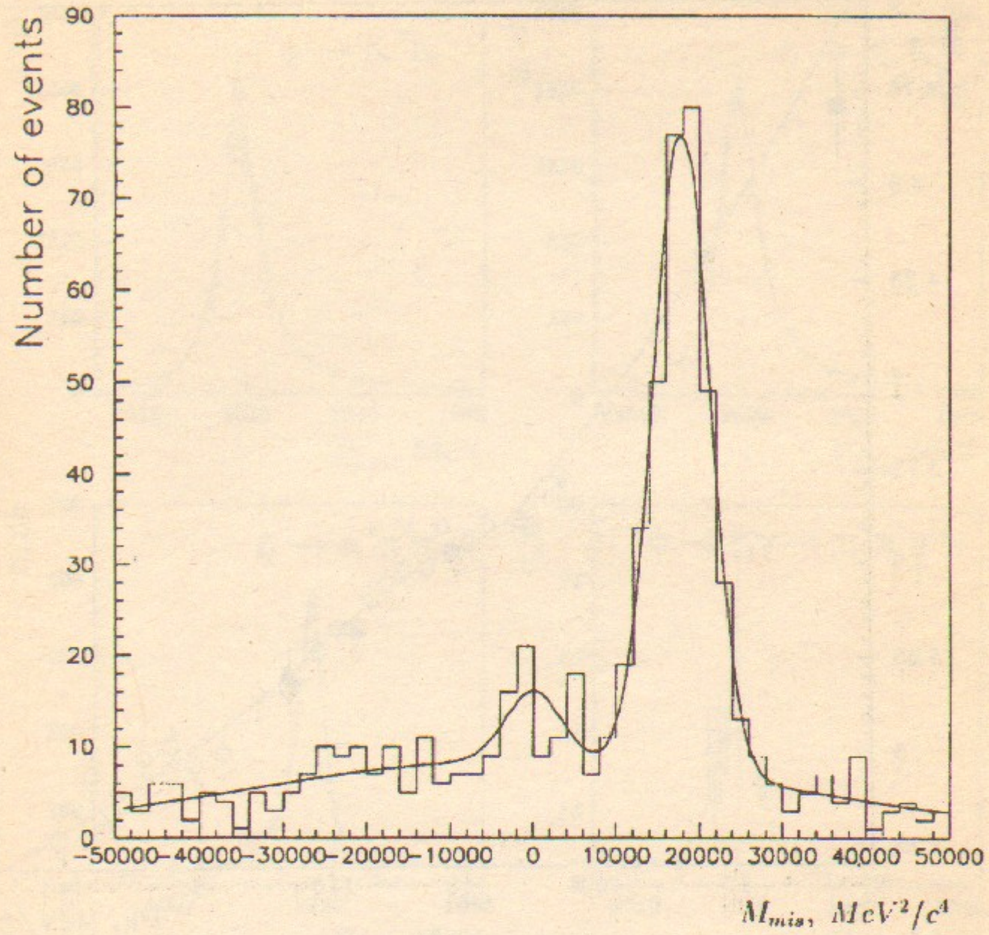

Figure 14. The missing mass of the three pion final state for $\eta\gamma$ candidates. The number of true events in the $\eta\gamma$ channel is obtained by subtracting the background under the π^0 peak.

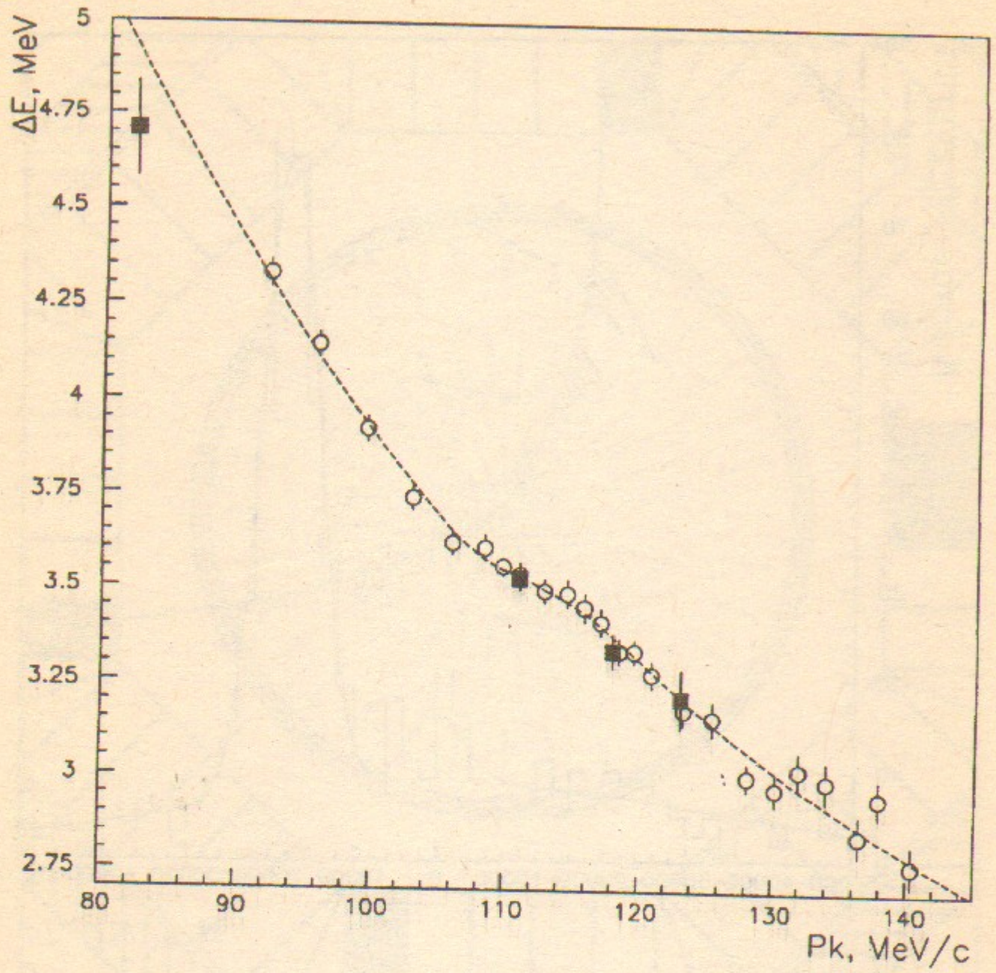

Figure 15. A correction curve for energy calculation by measured kaon momentum. Open circuses are from simulation, dark squares were obtained from resonance depolarization runs. Lines present fits before and after calibration.

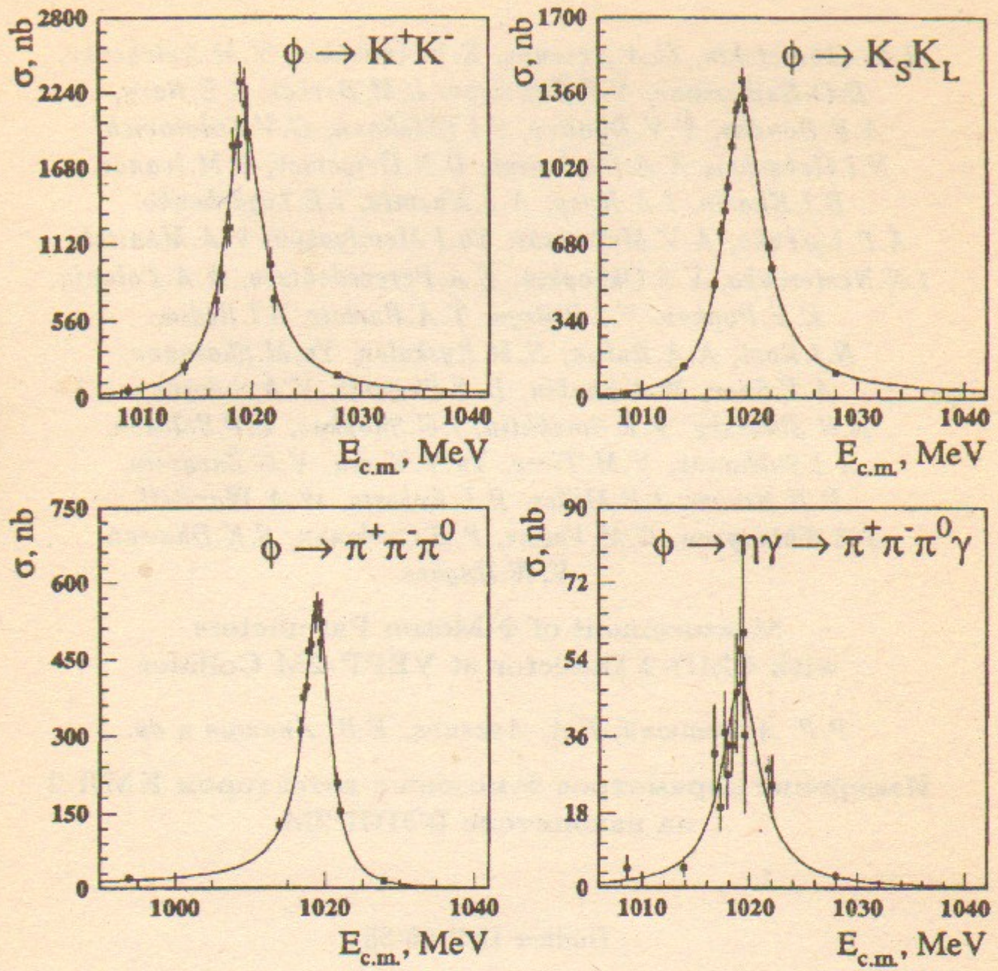

Figure 16. The ϕ-meson excitation curves for different channels.